Analysis of the longitudinal collective behavior in a 50 GeV × 50 GeV muon collider ring

Eun-San Kim[1], Andrew M. Sessler,[2] and Jonathan S. Wurtele[1,2]
[1]*Department of Physics, University of California, Berkeley, Berkeley, California 94720*
[2]*Lawrence Berkeley National Laboratory, Berkeley, California 94720*
(Received 13 January 1999; published 12 May 1999)

Simulations of the longitudinal instability in the 50 GeV × 50 GeV muon collider ring have been performed. Operation of the ring close to the slippage factor $\eta_1 \simeq 10^{-6}$, such that synchrotron motion is frozen, minimizes the need for rf to maintain the bunch length. However, there is still an energy spread due to the bunch wake. For design parameters of the ring, this induced energy is too large and must be controlled. This paper demonstrates that the bunch wake may be compensated for by two rf cavities with low rf voltages. These studies were made at the nominal design point, and sensitivities to errors were explored. It is seen that the small energy spread of the beam ($\delta E/E = 3 \times 10^{-5}$) in the 50 GeV × 50 GeV muon collider ring can be maintained during the 1000 turn lifetime of the muons. Controlled beam dynamics requires proper choice of rf parameters (rf voltage, rf frequency, and phase offset) for two cavities; these parameters depend on the ring design through the impedance, beam pipe radius, and momentum compaction. The simulation also shows that the computation of wake field using bins of variable width (each with a constant number of macroparticles in each bin) gives an accurate wake and also yields reduced computing time compared to an evaluation of the wake as the direct sum over the wakes of all preceding macroparticles. [S1098-4402(99)00042-7]

PACS numbers: 29.27.Bd

I. INTRODUCTION

In earlier papers [1–3], the longitudinal dynamics in muon collider rings was studied numerically with a multiparticle tracking code. The longitudinal force on the muons in the ring was modeled as consisting of two components, one from an rf cavity and the other from the wake field generated by the interaction between the beam and discontinuities of components in the ring. The wake was approximated by a broadband impedance and muon decay was included. Several single bunch collective effects in a 2 TeV × 2 TeV muon collider ring were examined.

This paper presents investigations of the longitudinal dynamics in a 50 GeV × 50 GeV muon collider ring. The critical design parameters of a 50 GeV × 50 GeV muon collider ring, from the viewpoint of collective effects, are (i) the bunch has a large charge ($N = 4 \times 10^{12}$), (ii) the bunch length is long ($\sigma_z = 13$ cm) compared to the pipe radius (a few centimeters), and (iii) the beam energy spread is very small ($\sigma_\delta = 3 \times 10^{-5}$), as is the slippage factor ($\eta_1 \simeq -10^{-6}$). The muon has a lifetime, $\tau_\mu \simeq 1.1$ ms at 50 GeV, corresponding to 1000 turns in the ring with a circumference (C) of 300 m [4]. The need to minimize rf voltage leads to $\eta_1 = -10^{-6}$ and a synchrotron oscillation period much longer than the storage time. These parameters are summarized in Table I. The small slippage over the storage time leads to dynamics similar to that in a linac. The large bunch charge induces, through the wake field, an undesirable head-to-tail energy spread. Maintaining an intense beam with a low energy spread provides a challenge to the ring design.

In this paper, we present a means of controlling the longitudinal dynamics in the 50 GeV muon collider ring. That is, to limit rf, one operates the ring close to the transition ($\eta_1 = 10^{-6}$) such that the synchrotron motion is frozen in the storage time, and uses two rf cavities to compensate for the ring impedance arising from beam and ring structures. In this way, the wake voltage resulting from the intense bunch is canceled out by the two rf voltages. Since the beam intensity decreases due to the muon decay, rf voltages must also vary in time.

The utility of the simulation depends on the ability to calculate a sufficiently accurate wake without excessive computation. We have implemented a binning scheme to calculate the wake. Various approaches to accurately describe wake fields have been implemented in several simulations [5,6]. In the simulation for a 2 TeV muon collider ring, with a characteristic bunch frequency ($c/\sigma_z \approx 100$ GHz) higher than the resonant frequency used in the broadband impedance model, the wake field was obtained by using a δ wake function evaluated for

TABLE I. Parameters of the 50 GeV muon collider ring.

Beam energy (E_0)	50 GeV
Muons per bunch (N)	4×10^{12}
Circumference (C)	300 m
Energy spread (σ_δ)	3×10^{-5}
Bunch length (σ_z)	13 cm
Slippage factors (η_1, η_2, η_3)	$\eta_1 = -1 \times 10^{-6}$, $\eta_2 < 3$, $\eta_3 \lesssim 1000$
Beam pipe radius (b_{pipe})	3 cm
Revolution period (T_0)	1 μs
Synchrotron tune (ν_s)	5.1×10^{-6}

1000 macroparticles [1–3]. This method is impractical (requiring too many macroparticles) for the 50 GeV muon collider ring, where, in contrast to the 2 TeV design, the characteristic bunch frequency is much less than the resonant wake frequency.

In the present code, the wake is calculated by summing the wakes from bins of variable bin width in front of the particle and δ wakes from preceding particles in the same bin. We performed tests for this method to calculate wake, and found that it gives the desired accuracy and a substantial reduction in computing time when compared to the wake calculation using unbinned macroparticles. Using these techniques, we demonstrate stable longitudinal beam dynamics for the required design parameters of a muon collider Higgs factory.

This paper is organized as follows: In Sec. II the computation of the wake field model and macroparticle equations are derived. An example in which the bunch wake is compensated for by one and two rf cavities is presented in Sec. III. Section IV is devoted to sensitivity studies. A discussion and our conclusions are given in Sec. V.

II. THE COMPUTATION OF THE WAKE FIELD AND MACROPARTICLE EQUATIONS

The wake generated by a beam interacting with discontinuities of components in the ring is approximated by a broadband impedance with quality factor of the order of unity. The longitudinal wake function $W_0'(z)$ for a broadband impedance is given by [7]

$$W_0'(z) = \begin{cases} 0, & \text{if } z > 0\,, \\ \alpha R_s, & \text{if } z = 0\,, \\ 2\alpha R_s \exp(\alpha z/c)\,(\cos\frac{\bar{\omega} z}{c} + \frac{\alpha}{\bar{\omega}}\sin\frac{\bar{\omega} z}{c}), & \text{if } z < 0\,, \end{cases} \tag{1}$$

where $\alpha = \omega_R/2Q$, $\bar{\omega} = \sqrt{w_R^2 - \alpha^2}$, $Q = R_s\sqrt{C/L}$ is the quality factor, $w_R = 1/\sqrt{LC}$ is the resonant frequency, and R_s is the shunt impedance. For the broadband model, $Q = 1$ and $\omega_R = c/b$, where b is the vacuum pipe radius. The more common impedance $Z_\parallel/n_h = (2\pi b/C)R_s$. Here C is the ring circumference and n_h is the harmonic number.

In the earlier simulations [1–3], the wake field $W(z_i)$ at the ith macroparticle on any turn n was calculated as a sum of δ wake functions $W_0'(z(n))$,

$$W(z_i(n)) = -\frac{N_b r_0}{N_p \gamma} \sum_j^{z_i<z_j} W_0'(z_i(n) - z_j(n)) - \frac{N_b r_0}{N_p \gamma} W_0'(0)\,, \tag{2}$$

where N_b is the number of particles in a bunch, N_p is the number of macroparticles, $\gamma = E_0/m_\mu c^2$, and $r_0 = e^2/m_\mu c^2$. The second term in Eq. (2) is the wake generated by the macroparticle itself. In trying to obtain an accurate wake field by use of Eq. (2), beams with long bunch length require many macroparticles. Since the number of operations to evaluate Eq. (2) is proportional to N_p^2, this method is less desirable with long bunches.

To reduce the computing time, we applied the following method for wake calculations: First, longitudinal positions of the macroparticles are binned with a constant number of particles in each bin. This results in bins of variable bin width. The position of each bin is given by the average position of the macroparticles inside the bin. The wake from macroparticles in preceding bins is calculated as arising from a single macroparticle (with properly enhanced charge) located at that bin position. Second, the interaction between macroparticles existing in the same bin is included as δ-function wakes. That is, the wake felt by a macroparticle in the ith bin is approximated first by calculating the sum of the averaged wakes from macroparticles in each preceding bin [the first term in the right-hand side of Eq. (3)], and then adding the individual wakes from the preceding macroparticles in the same bin [second term in the right-hand side of Eq. (3)], and finally adding the wake generated by the macroparticle itself [third term in the right-hand side of Eq. (3)],

$$W(z_i(n)) = -\frac{N_b r_0}{N_p \gamma} \sum_j^{z_i(n)<z_j(n)} N_j W_0'(z_i(n) - z_j(n)) - \frac{N_b r_0}{N_p \gamma} \sum_j^{z_i(n)<z_j(n)} W_0'(z_i(n) - z_j(n)) - \frac{N_b r_0}{N_p \gamma} W_0'(0)\,, \tag{3}$$

where N_j is the number of macroparticles in the jth bin.

Calculation using Eq. (3) is more efficient than using Eq. (2). We used 2035 bins for 44 768 macroparticles in the simulation. The wake field that was thereby obtained showed good agreement with analytical results. The number of bins and macroparticles must be properly chosen, as they depend on ring parameters such as the bunch length and the radius of the beam pipe. The initial longitudinal coordinates of macroparticles are chosen to have a Gaussian distribution.

Macroparticles are tracked in phase space with equations of motion which include kicks by two rf cavities, a longitudinal wake kick, and a drift that depends on the momentum compaction. Each macroparticle i has position and energy coordinates (z_i, δ_i) and is tracked for 1000 turns. The longitudinal difference equations for the ith macroparticle at revolution number n is

TABLE II. rf cavity parameters for wake compensation.

	One cavity	Two cavities
rf frequency ($f_{\rm rf}$)	570 MHz	823 and 399 MHz
Harmonic number	570	823 and 399
rf voltage ($V_{\rm rf}$)	14.1 kV	4.26 and 12.12 kV
Phase offset (ϕ)	3.55 rad	3.755 and 3.415 rad

derived from its coordinates on turn $n-1$ by

$$\delta_i(n) = \delta_i(n-1) + K_{\rm rf}(n-1) + W(z_i(n)), \quad (4)$$

$$z_i(n) = z_i(n-1) + (\eta_1\delta + \eta_2\delta^2 + \eta_3\delta^3)C. \quad (5)$$

Here, z is the longitudinal coordinate with respect to the bunch center, $\delta = \delta P/P$ is the relative momentum error of the particle, η_1, η_2, η_3 are the linear and higher order momentum compaction parameters, and C is the circumference of the ring. The rf impulse $K_{\rm rf}(n-1)$ (a negative quantity) due to the two rf voltages is given by

$$K_{\rm rf}(n-1) = \frac{eV_{\rm rf1}e^{-\frac{T_0(n-1)}{\gamma\tau_\mu}}}{E_0}\sin\left(\frac{w_{\rm rf1}}{c}z_i + \phi_1\right) + \frac{eV_{\rm rf2}e^{-\frac{T_0(n-1)}{\gamma\tau_\mu}}}{E_0}\sin\left(\frac{w_{\rm rf2}}{c}z_i + \phi_2\right). \quad (6)$$

The rf voltages ($V_{\rm rf1}$ and $V_{\rm rf2}$), rf frequencies ($w_{\rm rf1}$ and $w_{\rm rf2}$), and rf phase offsets (ϕ_1 and ϕ_2) are chosen to compensate for the bunch wake. An example of rf parameters that compensate the wake, for the ring parameters of Table I, are shown in Table II. The factor $e^{-[T_0(n-1)/\gamma\tau_\mu]}$ in the rf voltages is introduced to compensate the decreasing beam intensity due to muon decay. Here, T_0 is the revolution period.

Numerical example of the compensation of the bunch wake

The synchrotron oscillations are almost frozen during the storage time by the small choice for η_1. The bunch wake, when uncompensated, causes serious beam energy spread. With two modest rf voltages, the energy spread can be avoided through compensation of the bunch wake. The ring parameters are those of Table I.

Figures 1(a) and 1(b) show the beam phase space after one turn and 1000 turns in the case that voltages are not applied to the two rf cavities ($V_{\rm rf1} = V_{\rm rf2} = 0$). It is seen that the phase space after 1000 turns is distorted by the bunch wake.

Figures 2(a) and 2(b) show the beam phase space after 1 turn and 1000 turns in the case that $V_{\rm rf1} \neq 0$ has been chosen to minimize the induced energy spread and $V_{\rm rf2} = 0$. The wake in the center of the bunch has been compensated, but, after 1000 turns, the tail particles gain or lose energy from the large rf kick at the longitudinal positions where the bunch wake becomes small. This can be understood from examination of Fig. 2(c), where the rf voltage [curve (1)], bunch wake voltage [curve (2)], and the resulting total voltage [curve (3)] are plotted after one turn. A similar plot, Fig. 2(d), shows the same curves after 1000 turns. The amplitude of the wakes are smaller since the muons have decayed and the rf voltage has been correspondingly reduced. The rf parameters are given in Table II, column 2.

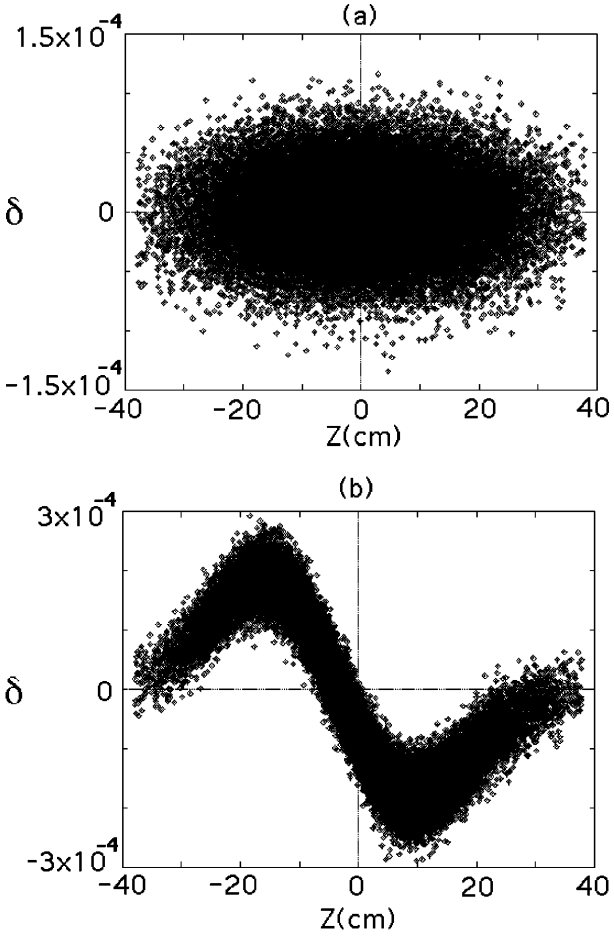

FIG. 1. The longitudinal beam phase space at (a) turn 1 and (b) turn 1000 when the rf voltages are not applied. The beam distribution after 1000 turns is distorted by the bunch wake. The initial energy spread was $\sigma_\delta = 1 \times 10^{-3}$, $\eta_1 = -1 \times 10^{-6}$, $V_{\rm rf1} = V_{\rm rf2} = 0$, and $|\frac{Z_\parallel}{n_h}| = 0.1\ \Omega$.

Figures 3(a) and 3(b) show the beam phase space after 1 turn and 1000 turns when both $V_{\rm rf1} \neq 0$ and $V_{\rm rf2} \neq 0$. The beam distribution after 1000 turns is not distorted by the sum of the rf voltages and the bunch wake and the beam distribution remain intact. Figure 3(c) shows the cancellation of the wake by the rf voltages. The rf parameters are given in Table II, column 3. We note that the bunch wake in the 50 GeV $\times$ 50 GeV muon collider ring can be compensated by very low rf voltages.

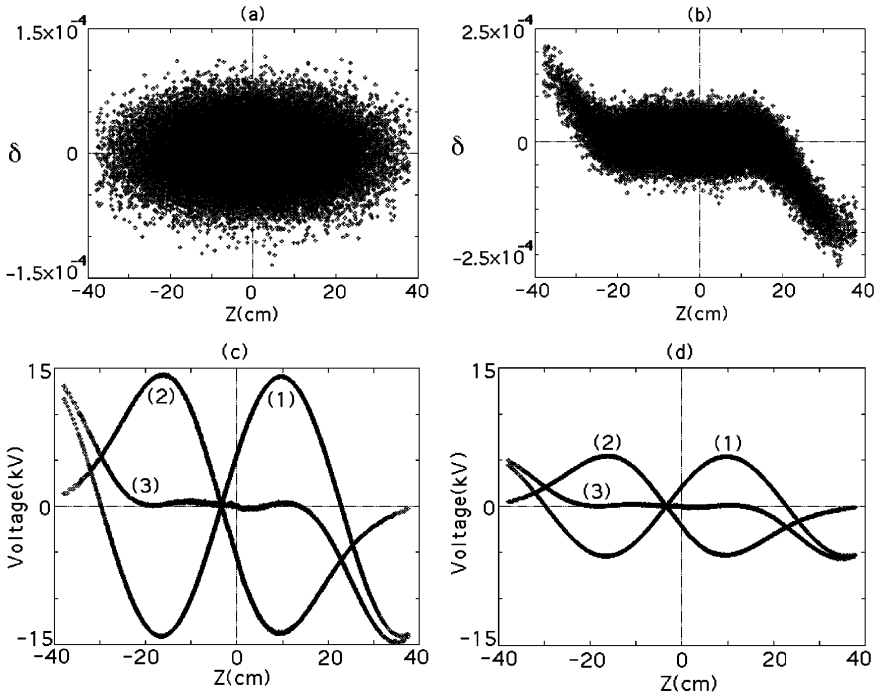

FIG. 2. The longitudinal beam phase space at (a) turn 1 and (b) turn 1000 with $V_{\mathrm{rf}1} = 14.1$ kV and $V_{\mathrm{rf}2} = 0$. (c) (turn 1) and (d) (turn 1000) show the voltages of the rf [curve (1)], the bunch wake [curve (2)], and total voltage across the bunch [curve (3)]. The bunch wake is partly compensated for by the rf voltage, but the tails of the bunch are distorted by the rf. The difference between (c) and (d) is a consequence of the decay of the muons and the rf voltage. The parameters are $\sigma_\delta = 3 \times 10^{-5}$, $\eta_1 = -1 \times 10^{-6}$, $|\frac{Z_\parallel}{n_h}| = 0.1\ \Omega$, $V_{\mathrm{rf}1} = 14.1$ kV, $V_{\mathrm{rf}2} = 0$, $f_{\mathrm{rf}1} = 570$ MHz, and $\phi_1 = 3.55$ rad.

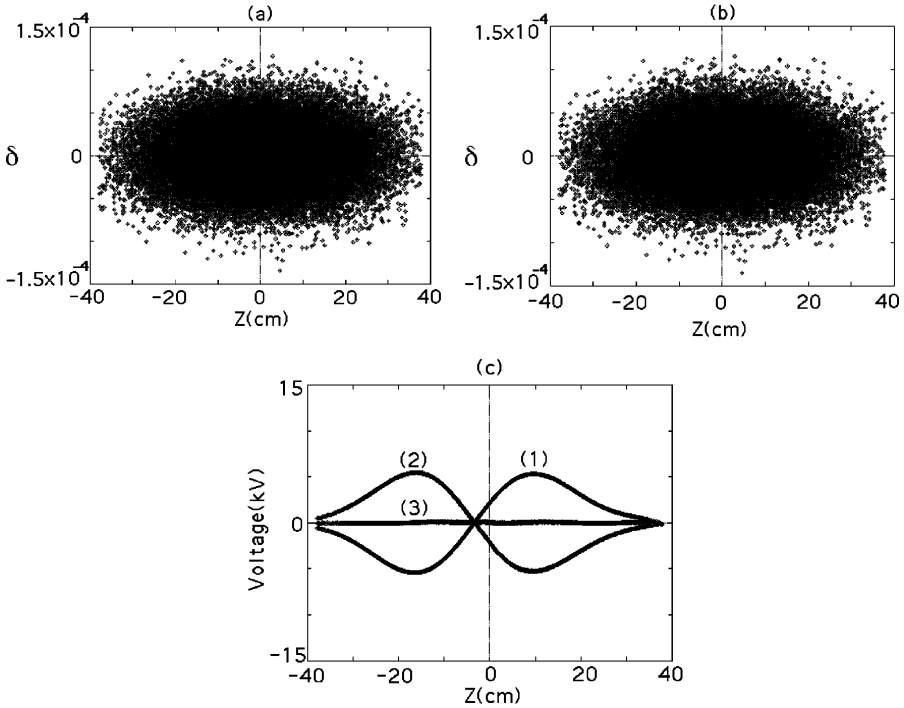

FIG. 3. The longitudinal beam phase space after 1 turn (a) and 1000 turns (b) when two rf voltages are applied. (c) shows voltages due to the two rf cavities [curve (1)], the bunch wake [curve (2)], and the net voltage [curve (3)] after 1000 turns. The bunch wake is well compensated by the two rf cavities, with $V_{\mathrm{rf}1} = 4.26$ kV, $V_{\mathrm{rf}2} = 12.12$ kV, $\phi_1 = 3.755$ rad, $\phi_2 = 3.415$ rad, $f_{\mathrm{rf}1} = 823$ MHz, and $f_{\mathrm{rf}2} = 399$ MHz. $\sigma_\delta = 3 \times 10^{-5}$, $\eta_1 = -1 \times 10^{-6}$, and $|\frac{Z_\parallel}{n_h}| = 0.1\ \Omega$.

While this cancellation is good, the choice of rf parameters is affected by bunch length, bunch intensity, beam pipe radius, and shunt impedance. Thus, one needs to consider sensitivity to ring parameters.

III. SENSITIVITY STUDIES OF LONGITUDINAL DYNAMICS

In this section, we study the sensitivity of our solution to variations in critical ring parameters.

A. Sensitivity to beam current and $|\frac{Z_0^{\parallel}}{n_h}|$

Figures 4(a)–4(d) show the beam phase space after 1000 turns with beam current varying from its design value by -10%, -5%, $+5\%$, and $+10\%$, respectively. The rf parameters are fixed, as given in Table II, column 3. The energy spread has increased roughly 8% for Figs. 4(a) and 4(d), and 2% for Figs. 4(b) and 4(c).

Figures 5(a)–5(d) show the beam phase space after 1000 turns for variations of the impedance: $|\frac{Z_0^{\parallel}}{n_h}| = 0.1\ \Omega$, $0.5\ \Omega$, $0.7\ \Omega$, and $1\ \Omega$, respectively. Here, $|\frac{Z_0^{\parallel}}{n_h}|$ is related to the shunt impedance as $R_s = |\frac{Z_{\parallel}}{n_h}|\frac{w_r}{w_0} = |\frac{Z_{\parallel}}{n_h}|\frac{C}{2\pi b}$. Voltages in the rf cavities are varied proportionally to the magnitude of $|\frac{Z_0^{\parallel}}{n_h}|$. The potential well distortion due to the bunch wake increases with $|\frac{Z_0^{\parallel}}{n_h}|$ and becomes quite noticeable at $1\ \Omega$.

Figures 6(a) and 6(b) show the beam distributions after 1000 turns for radii of the beam pipe (b) of 3 and 1.76 cm, respectively. The resonant frequency of the broadband impedance is $w_r \simeq c/b$, and the shunt impedance is then 159 Ω and 270 Ω for $b = 3$ cm and $b = 1.76$ cm, respectively. Figures 6(a) and 6(b) have $|\frac{Z_0^{\parallel}}{n_h}| = 0.1\ \Omega$. The voltages of the two rf cavities in Figs. 6(a) and 6(b) are varied corresponding to the magnitude of R_s.

B. Dependence of longitudinal dynamics on σ_δ and η_1, η_2, η_3

Figure 7 shows the beam phase space after 1000 turns for several values of η_1 and σ_δ. σ_δ denotes initial energy spread. Here, only one rf voltage is used to compensate for bunch wake. The rf parameters are given in Table II, column 2. In Figure 7(a), $\sigma_\delta = 0.001$ and $\eta_1 = -1 \times 10^{-6}$ and the distribution is essentially unchanged over 1000 turns. Figure 7(b) corresponds to $\sigma_\delta = 3 \times 10^{-5}$ and $\eta_1 = -1 \times 10^{-6}$. This distribution shows tails which are distorted by the large rf voltage [Fig. 2(b)].

In the calculations for previous figures, and for Fig. 7, we have had $\eta_2 = \eta_3 = 0$, and the equation of motion [from Eqs. (4)–(6)],

$$z' = \eta_1 \delta(s), \tag{7}$$

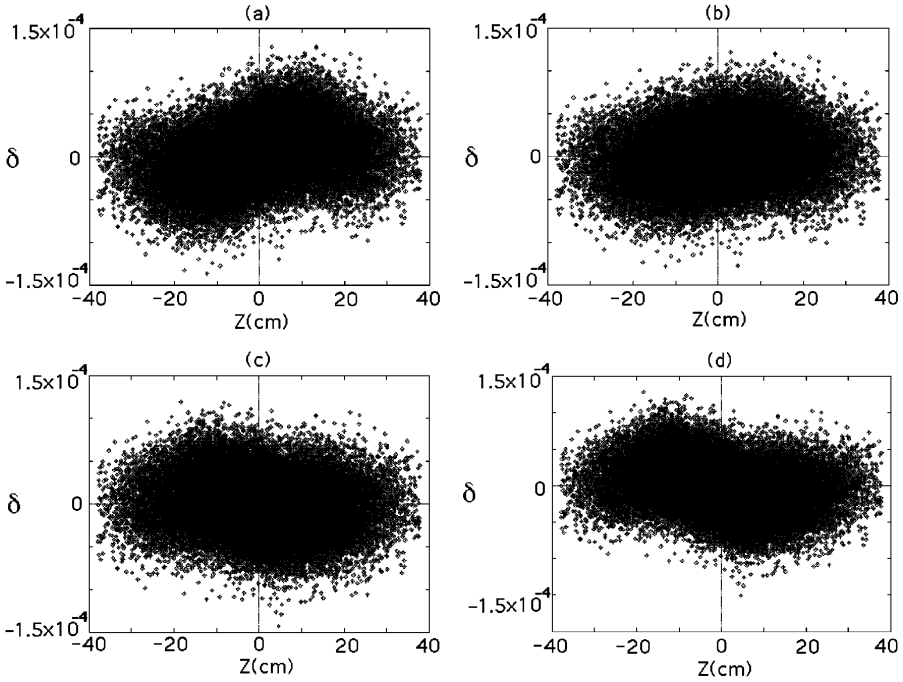

FIG. 4. The sensitivity of the longitudinal beam phase space to the variations of the bunch current. The number of particles in a bunch is varied from the design value by -10%, -5%, $+5\%$, and $+10\%$ in (a)–(d), respectively. Two rf voltages are held fixed at the values used in Fig. 3, in (a)–(d). In addition, $\sigma_\delta = 3 \times 10^{-5}$, $\eta_1 = -1 \times 10^{-6}$, and $|\frac{Z_{\parallel}}{n_h}| = 0.1\ \Omega$.

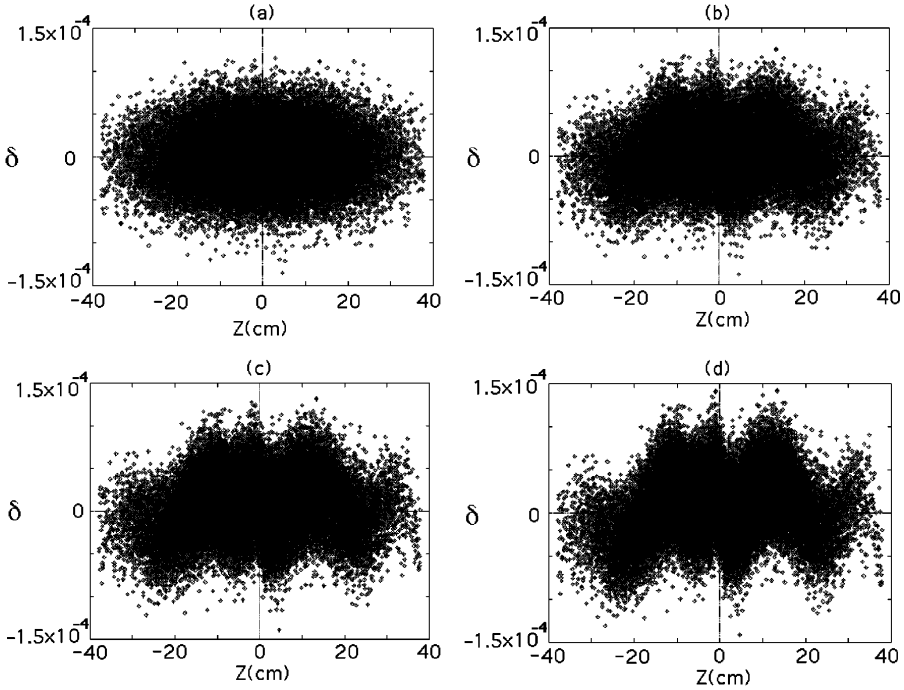

FIG. 5. The sensitivity of the longitudinal beam phase space to the variations of $|\frac{Z_0^{\parallel}}{n}|$. $|\frac{Z_0^{\parallel}}{n}|$ in (a)–(d) are 0.1, 0.5, 0.7, and 1 Ω, respectively, and $\sigma_\delta = 3 \times 10^{-5}$ and $\eta_1 = -1 \times 10^{-6}$. The voltages in the rf cavities are scaled linearly with $|\frac{Z_0^{\parallel}}{n_h}|$ to compensate for the bunch wake. The effects of imperfect cancellation become more apparent at the higher impedances.

$$\delta'(s) = \frac{eV_{\mathrm{rf}1}(z)e^{-\frac{T_0(n-1)}{\gamma\tau\mu}} + eV_{\mathrm{rf}2}(z)e^{-\frac{T_0(n-1)}{\gamma\tau\mu}}}{CE} + \frac{N_b r_0}{N_p \gamma C}\int_{z'}^{\infty} W_0(z - z')\rho(z')\,dz', \qquad (8)$$

where $z' = \frac{dz}{ds}$, $\delta' = \frac{d\delta}{ds}$, and s is the distance traveled in the ring.

Figure 7(c) shows the beam phase space with $\sigma_\delta = 0.001$ and $\eta_1 = -1 \times 10^{-2}$. When $\delta'(s)$ integrated over 10^3 turns is small compared to σ_δ, the motion of a particle is determined by the magnitude of η_1. The large slippage dominates the motion and leads to streaming in z motion, as is seen in Fig. 7(c). Figure 7(d) shows the beam phase space in the case of $\sigma_\delta = 3 \times 10^{-5}$ and $\eta_1 = -1 \times 10^{-2}$. In the case of large η_1, and small energy spread, the dynamics is significantly more complicated, as shown in Fig. 7(d). The resultant phase space after 10^3 turns is summarized as a function of (η_1, σ_δ) in Fig. 7(e).

Figures 8(a)–8(d) show results for parameters identical to those of Figs. 7(a)–7(d), with the exception that the rf now has two cavities, as given in Table II, column 3. Clearly, the two-voltage compensation reduces the phase space distortions of the beam for the parameters of

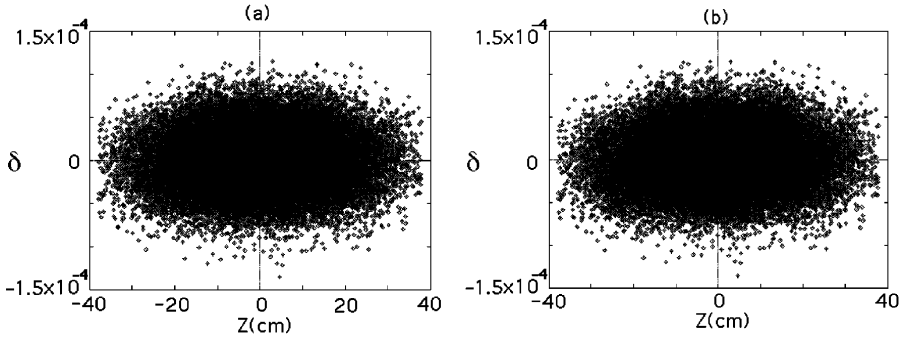

FIG. 6. The longitudinal beam phase space for two values of the beam pipe radius 3.0 cm in (a) and 1.76 cm in (b). The resulting resonant frequency w_r of the broadband impedance in (a) and (b) is 10 and 16.9 GHz, respectively. With appropriate adjustment of the two rf cavities, the compensation scheme is seen to work. In both figures, $\sigma_\delta = 3 \times 10^{-5}$, $\eta_1 = -1 \times 10^{-6}$, and $|\frac{Z^{\parallel}}{n_h}| = 0.1\ \Omega$.

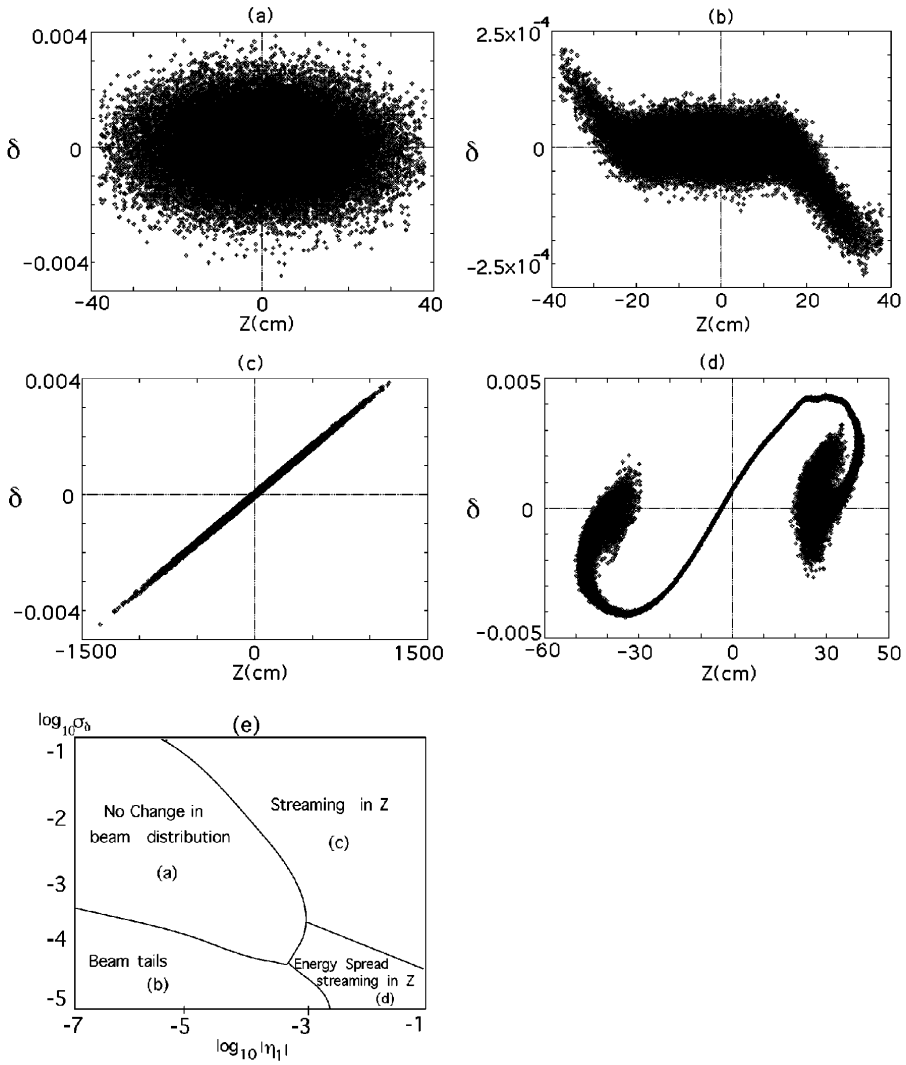

FIG. 7. The longitudinal phase space after 1000 turns for different values of σ_δ and η_1. One rf voltage is used to compensate for the bunch wake (given by Table II, column 2). In (a) $\sigma_\delta = 0.001$ and $\eta_1 = -1 \times 10^{-6}$, (b) $\sigma_\delta = 3 \times 10^{-5}$, and $\eta_1 = -1 \times 10^{-6}$, (c) $\sigma_\delta = 0.001$ and $\eta_1 = -1 \times 10^{-2}$, (d) $\sigma_\delta = 3 \times 10^{-5}$, and $\eta_1 = -1 \times 10^{-2}$. (e) gives a summary of the beam dynamics in σ_δ and η_1 parameter space. This parameter space shows the parameter when one rf voltage is used to compensate for bunch wake. In each figure, $|\frac{Z_\parallel}{n_h}| = 0.1\ \Omega$.

Figs. 7(a), 7(b), and 7(d). The motion in Figs. 7(c) and 8(c) is dominated by slippage, and the rf does not affect the dynamics. In summary, two rf cavities can be used to remove the beam tail of the (b) region of Fig. 7(e) and the energy spread of the (d) region of Fig. 7(e).

Figure 9 shows the beam phase space after 1000 turns with variation of η_2 and fixed $\eta_1 = -1 \times 10^{-6}$ and $\eta_3 = 0$. Other parameters are as in Table I and Table II, column 3. Now, the z' equation includes a nonlinear term

$$z' = [\eta_1 + \eta_2 \delta(s)]\delta(s). \tag{9}$$

With two rf cavities used to compensate the bunch wake, the energy does not show significant change after 1000 turns and the motion is a nonlinear streaming described roughly by Eq. (9) with the energies taken as their initial values. We see this in Fig. 9 where the energy spread of the macroparticles is basically unchanged. The nonlinearity of the streaming is noticeable in Fig. 9(c) where, for particles with $\eta_2 > \eta_1/\delta(s)$, the streaming direction is independent of the sign of δ, but depends quadratically on its magnitude and on the sign of η_2. The behavior of the phase space parameterized by η_2 and σ_δ is summarized in Fig. 9(d).

Figure 10 shows the beam phase space after 1000 turns with variation of η_3 and fixed $\eta_1 = -1 \times 10^{-6}$ and $\eta_2 = 0$. Other parameters are as in Table I and Table II, column 3. The energy evolution is small due to good compensation, and the position evolves according to

$$z' = [\eta_1 + \eta_3 \delta^2(s)]\delta(s), \tag{10}$$

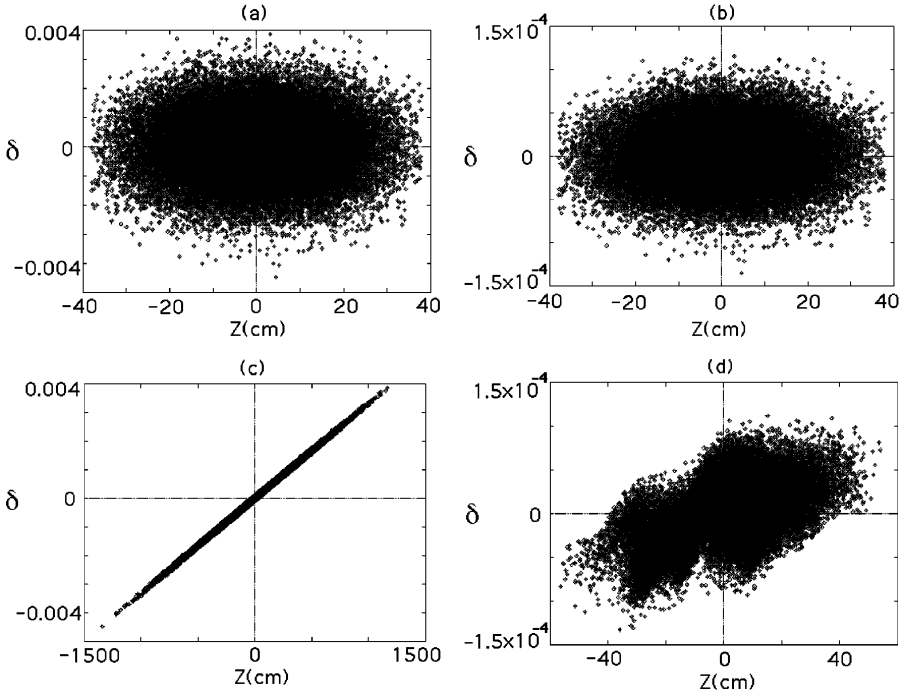

FIG. 8. The longitudinal phase space after 1000 turns for different values of σ_δ and η_1, with, in contrast to Figs. 7(a)–7(d), two rf cavities used to compensate the bunch wake. The rf corresponds to Table II, column 3. The situation is improved when two rf cavities are used, as shown in (a), (b), and (d). The values of σ_δ and η_1 in (a)–(d) correspond to their respective values in Figs. 7(a)–7(d). The motion in Figs. 7(c) and 8(c) is dominated by slippage, and the rf does not affect the dynamics. In each figure, $|\frac{Z_\parallel}{n_h}| = 0.1\ \Omega$.

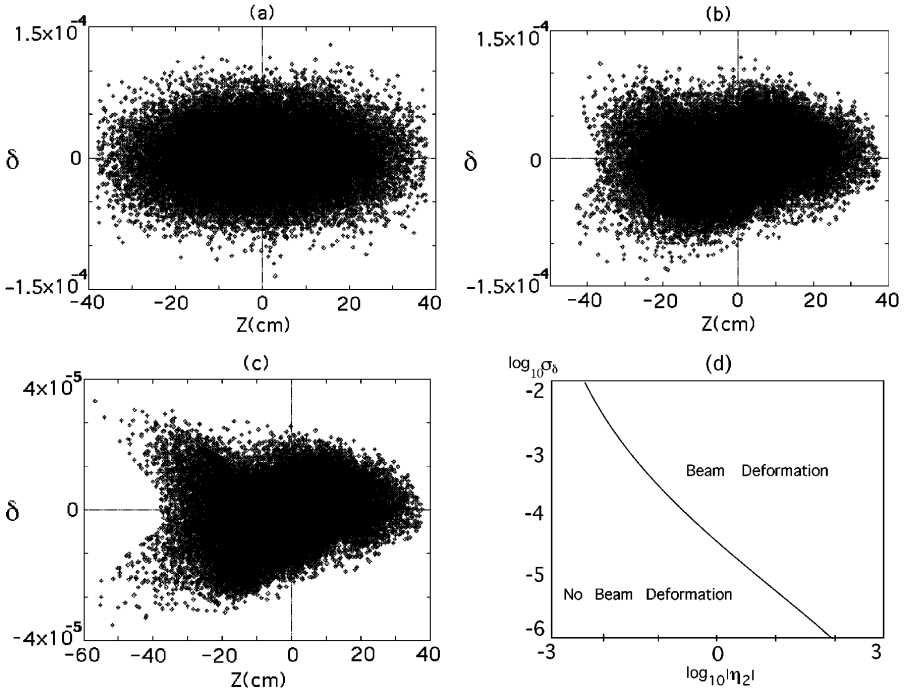

FIG. 9. The longitudinal phase space after 1000 turns for (a) $\eta_2 = 3$, (b) $\eta_2 = 50$, and (c) $\eta_2 = 100$. Two cavities are used to compensate for bunch wake. (d) shows beam dynamics in the σ_δ and η_3 parameter space. The right upper parameter space shows the beam streaming of positive or negative z direction, depending on the sign of η_2. Here, $\eta_1 = -1 \times 10^{-6}$, $\eta_3 = 0$, $\sigma_\delta = 3 \times 10^{-5}$, and $|\frac{Z_\parallel}{n}| = 0.1\ \Omega$.

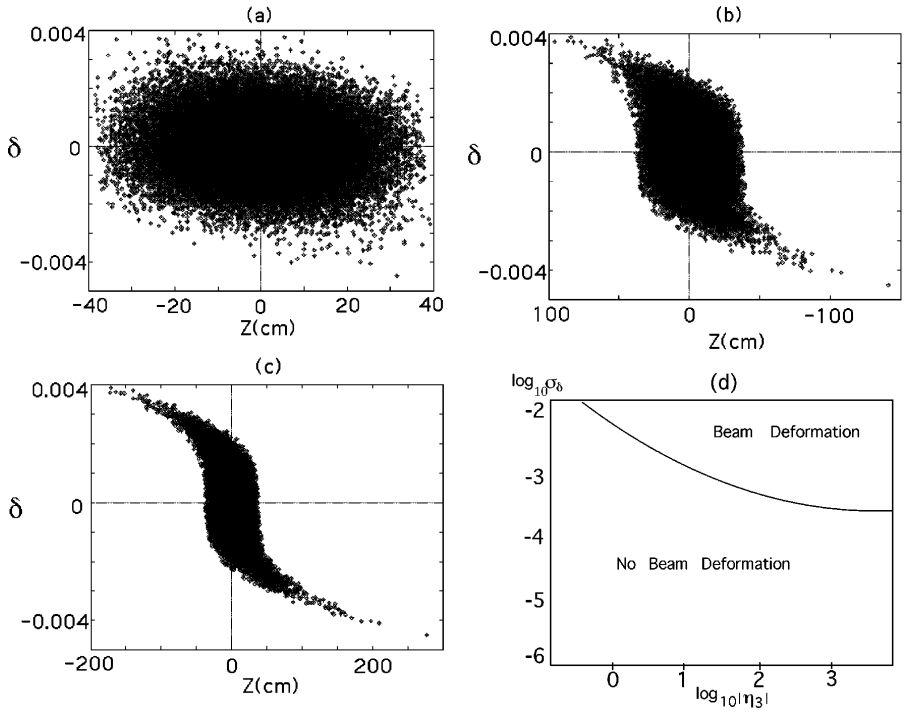

FIG. 10. The longitudinal phase space after 1000 turns for (a) $\eta_3 = 10$, (b) $\eta_3 = 50$, and (c) $\eta_3 = 100$. Two cavities are used to compensate for bunch wake. $\sigma_\delta = 3 \times 10^{-5}$, $\eta_1 = -1 \times 10^{-6}$, $\eta_2 = 0$, and $|\frac{Z_\parallel}{n_h}| = 0.1\ \Omega$. (d) shows beam dynamics in the σ_δ and η_3 parameter space. The right upper parameter space shows the beam streaming in the positive or negative z direction.

where the energy can be taken roughly to be fixed at its initial value. The nonlinear coefficient η_3 becomes important when $\eta_3 > \eta_1/\delta^2(s)$. For positive η_3, the particles with negative δ move to the positive z direction and the particles with positive δ move to the negative z direction. The parameter space for varying η_3 and σ_δ is summarized in Fig. 10(d).

IV. CONCLUSION

Longitudinal motion in the 50 GeV × 50 GeV muon collider ring is investigated with a multiparticle tracking code. A binning scheme is used to enhance the computational efficiency of the simulation and muon decay is included. The operation of a ring with small η_1, so that the synchrotron oscillation is frozen during the storage time, and with the bunch wake compensated by two low rf cavities, is studied. The wake was modeled with a broadband impedance.

The longitudinal dynamics is seen to be controllable with the proper choice of rf parameters. One cavity can be used to control the motion of the core of the bunch, while a second controls the tails. We studied the role played by important ring parameters in the longitudinal dynamics. Longitudinal motion with compensation of the wake was studied with various slippage factors (η_1, η_2, and η_3) and values were found above which the bunch lengthened. It was also shown that η_1, η_2, and η_3 each show different characteristic behaviors. The sensitivity of the compensation scheme to variations in ring parameters was examined.

ACKNOWLEDGMENT

This work was supported by the U.S. Department of Energy under Contracts No. DE-FG-03-95ER40936 and No. DE-AC03-76SF00098.

[1] W.-H. Cheng, A. M. Sessler, and J. S. Wurtele, in *Proceedings of the 5th European Particle Accelerator Conference, Barcelona Spain, 1996* (Institute of Physics, Bristol, UK, 1996), pp. 1081–1083.
[2] W.-H. Cheng, A. M. Sessler, and J. S. Wurtele, LBL Report No. LBL-40251, 1997.
[3] W.-H. Cheng, A. M. Sessler, and J. S. Wurtele, LBL Report No. LBL-40224, 1998.
[4] C. M. Ankenbrandt *et al.* (to be published).
[5] K. Bane and K. Oide, in *Proceedings of the 1993 IEEE Particle Accelerator Conference, Washington DC, 1993* (IEEE, Piscataway, NJ, 1993), p. 3339.
[6] D. Brandt, CERN Report No. CERN/ISR-TH/82-09, 1982.
[7] A. W. Chao, *Physics of Collective Instabilities in High Energy Accelerators* (Wiley, New York, 1993).